Research on Chemical Intermediates, Vol.19, No.1, pp. 31-57 (1993)

LUMINESCENCE PROPERTIES OF CU^+ IN ZEOLITES. IN SITU STUDY OF THIN LAYERS

G. CALZAFERRI*, R. GIOVANOLI and I. KAMBER
Institute for Inorganic and Physical Chemistry, University of Berne, CH-3000 Berne 9, Switzerland

V. SHKLOVER
Institute of Crystallography and Petrography, ETH-Zentrum, CH-8092 Zürich, Switzerland

R. NESPER
Institute of Inorganic Chemistry, ETH-Zentrum, CH-8092 Zürich, Switzerland

Received 20 November 1992; accepted 4 December 1992

Abstract--Thin layers of zeolites A and X with different alkali cations partially exchanged by Cu^{2+} have been prepared on glass or quartz supports. X-ray powder diffraction of these samples yield surprisingly good patterns. A sample chamber for *in situ* luminescence spectroscopy is described which allows the monitoring of the luminescence of Cu^+ during the reduction of Cu^{2+}, as a function of the reducing gas, the pretreatment, the water content and other parameters. Such luminescence measurements have shown that Cu^{2+} is reduced with CO and with H_2 to some extent already at room temperature. The first electronic absorption observed in Cu^+ zeolites occurs in the near UV and is attributed to a Cu^+ ($4s^*$) ← zeolite-oxygen lone-pair LMCT transition. Out of this charge transfer state luminescence occurs with a large Stokes shift which is caused by structural relaxation. The position of the emission depends on the alkali co-cations. In zeolite A this shift is correlated with the size of the unit cell. No correlation has been observed in zeolite X. The luminescence intensity is remarkably influenced by the degree of hydration going through a pronounced maximum that depends on the co-cation and on the type of zeolite.

INTRODUCTION

The strong green luminescence of Cu^+ zeolites provides information on the coordination of the Cu^+ ion which in this environment is stable towards disproportionation and often also towards oxidation. This luminescence has been used to study the reactivity of Cu^+ towards NO, CO, unsaturated hydrocarbons, and other compounds. Attempts to understand the microenvironments of Cu^+ in the zeolites A, X and Y lead to the conclusion that its electronic structure can be described by crystal field theory arguments [1,2]. As a consequence absorption as well as emission spectra were interpreted as transitions between states resulting from the $3d^94s^1$ and the $3d^{10}$ configuration of Cu^+ in trigonal coordination. The electronic structure of the zeolite was not taken into account, however, in this interpretation. We and others found that this picture is not valid and that

the first electronic absorption is due to a Cu^+ ←zeolite-oxygen lone-pair LMCT transition [3-6]. This was supported by the finding that the HOMO region of the zeolites which consists of oxygen lone pairs closely spaced in energy lies at about -10.7 eV. This is high in comparison to the first ionization energy of the water molecule, observed at 12.6 eV [7,8]. More detailed information on the properties, the coordination, and the location of Cu^+ in the various zeolites would help to improve our understanding of these materials that have great interest as catalysts or photocatalysts for reactions such as oxidation of hydrocarbons, the oxidation of ethylene to acetaldehyde [9], the oxidation of ethanol either to ethene or to CO_2 [10], the reduction of NO [11-19], or the oxidation of CO [14,20,21]. Despite this, no X-ray structure of Cu^+-zeolite seems to be available at the present time while X-ray data on Cu^{2+} zeolites have been published [22-24]. The main efforts in determining the location of copper ions were concentrated on EPR and ESE studies of Cu^{2+} in zeolites A [25-33] and X or Y [27,29,33-36]. It seems, however, questionable to make conclusions based on the location of Cu^+ in zeolites based on the known sites of Cu^{2+} because of the large differences of the ionic radii between Cu^{2+} (0.72 Å) and Cu^+ (0.96 Å), because of differences in the form of coordination of polyhedra of Cu^{2+} and Cu^+, and perhaps also because Cu^{2+} is prone to a static Jahn-Teller distortion.

A correlation between the position of the luminescence maximum and the distance between the layers has been reported for Cu^+-β″-alumina [37]. β″-alumina is layered aluminium oxide. The distance between the layers influences the interaction distance between the layer oxygens and the Cu^+ and therefore the electronic structure of the system. One might expect to find a similar behaviour of Cu^+ in zeolites. It should be more pronounced in the more compact zeolite A than, for example, in a more loose lattice such as zeolite X. This is supported by extended-Hückel calculations which show that decreasing the zeolite oxygen to Cu^+ distance causes increasing zeolite HOMO to $Cu^+(4s^*)$ splitting because of the antibonding interaction between the zeolite oxygen lone pairs and the 4s orbital of the copper [4]. Zeolites containing different alkali cations are expected to differ slightly in their lattice parameters and can therefore be used to check this hyypothesis. *In situ* luminescence spectroscopy on Cu^+ zeolite pellets have shown that the water content strongly affects the emission intensity of Cu^+-A and Cu^+-X zeolites [38]. It was, however, not possible to investigate the effect in more detail on these relatively thick samples probably because of non-homogeneity of the water content of the pellets. We shall show that this problem disappears by using very thin layers of zeolite crystallites. These layers enable us to achieve more homogeneous samples. They also allow us to investigate in more detail the influence of CO and H_2 as reducing gases on the preparation of the Cu^+ samples from the Cu^{2+} zeolites and on the influence of the alkali co-cations. It is remarkable that high quality X-ray powder patterns of such layers can be measured thus allowing their characterization.

EXPERIMENTAL

Sample Preparation

Commercially available zeolite A (Baylit T, Bayer AG) and zeolite X (Union Carbide) in their Na^+ form were used as starting materials. Their composition is $Na_{12}[(AlO_2)_{12}(SiO_2)_{12}]\cdot 27H_2O$ for zeolite A and $Na_{86}[(AlO_2)_{86}(SiO_2)_{106}]\cdot 276H_2O$ for zeolite X according to the manufacturer.

Alkali zeolites. Samples with different alkali cations (Li^+, Na^+, K^+ and Cs^+), from here on referenced as co-cation, were prepared by ion exchange in aqueous dispersions at room temperature. Each exchange was performed three times with a solution containing an excess of the co-cation as chloride. After each step the zeolite was centrifuged off and washed several times with doubly distilled water. After the final exchange the zeolite was washed 5 times and then dried for 24 h at 60 °C. In the last washing solution no Cl^- could be detected using $AgNo_3$. The samples so prepared, are called Li^+-A, Na^+-A, ... Cs^+-X. According to Breck [39] complete exchange is achieved in all cases apart from the Cs^+ zeolites, where the degree of exchange is about 45% (zeolite A, 0.1 M, 25 °C) and 65% (zeolite X, 0.1 M, 25 °C). While the Na^+-X zeolite was washed three times with a NaCl solution and then with doubly distilled water, the Na^+-A zeolite was used as delivered by the manufacturer and we denote it as $(Na^+\text{-A})_{ut}$ (ut = untreated).

Copper (II) zeolites. Samples with different co-cations were partially exchanged with Cu^{2+} using dilute solutions containing the appropriate amount of $Cu(NO_3)_2\cdot 3H_2O$ (zeolite A) or $CuCl_2\cdot 2H_2O$ (zeolite X). Zeolite A is exchanged 2.5% by charge with the exception of Cs^+-A which is exchanged by only 1.1%. Zeolite X is exchanged 15% by charge. These samples will be referenced as LiCu-A, NaCu-A, ... CsCu-X. The chosen copper concentrations of 2.5% (zeolite A) and 15% (zeolite X) lead to maximum luminescence intensities in the case of Na^+ as co-cation [38]. At these low exchange levels the problem of collapsing zeolite framework can be ignored [1,40]. No special caution was taken to avoid formation of OH^- bridged, multinuclear Cu^{2+} complexes in or on the zeolite crystals. Such bridged Cu^{2+} complexes have been observed for several zeolites at higher Cu^{2+} loading than used by us or at high pH [17,22,41-44].

Thin layer preparation. The copper exchanged zeolites were functionalized with vinyl groups according to Calzaferri *et al.* [45,46]. The zeolites were dispersed by sonification in ethanol and triethoxyvinylsilane was added. The dispersions were vigorously stirred for 96 h under N_2. The functionalized zeolites were centrifuged off, washed several times with EtOH and dried at 60 °C. These samples are called vinyl-

LiCu-A, vinyl-NaCu-A, ... vinyl-CsCu-X. Thin layers were prepared by using dispersions containing 45 mg of the functionalized zeolite in 6 ml H_2O/CH_3CN (1:1 by volume). 20 μl of the dispersion were dripped on freshly cleaned quartz plates. A mask of scotch tape with a hole of 5 mm diameter was used to obtain nicely shaped samples. After evaporating the solvent very slowly the vinyl groups were illuminated for 10 min using a 8 W/255 nm lamp. We do not know to what extent photopolymerization of the vinyl groups takes place [47]. The sample thickness was estimated to be 4.0 μm based on the amount of zeolite used. From the size of the zeolite particles (A ~ 2 μm and X ~ 1-2 μm) specified by the manufacturer the layers are estimated to be about two crystallites thick. The name polygrain layers seems therefore appropriate in comparison to the dense *monograin* layers of zeolite A on Pt electrodes [45]. Larger and thicker samples for X-ray powder diffraction measurements were prepared on glass using 100 μl of the dispersion and a mask with a 10 mm hole. The thickness of these samples is approximately 5.0 μm.

Copper (I)-zeolites. The Cu^{2+} samples are reduced *in situ* prior to the luminescence measurements with either H_2 or CO according to the overall reactions (1) or (2), respectively.

$$Cu_n^{2+}Na_{N-2n}^{+}[Z,mH_2O] + \frac{n}{2}H_2 \rightarrow Cu_n^{+}H_n^{+}Na_{N-2n}^{+}[Z,mH_2O] \quad (1)$$

$$Cu_n^{2+}Na_{N-2n}^{+}[Z,mH_2O] + \frac{n}{2}CO \rightarrow Cu_n^{+}H_n^{+}Na_{N-2n}^{+}[Z,(m-\frac{n}{2})H_2O] + \frac{n}{2}CO_2 \quad (2)$$

$[Z,mH_2O]$ represents the partially hydrated zeolite framework while *N* stands for the total number of charges per pseudo unit cell, *i.e.* N = 12 for zeolite A and N = 86 for zeolite X. Note that the reduction with H_2 does not affect the water content of the zeolite while the water molecules are the oxygen and the proton source in the reaction with CO. The following general procedure to prepare Cu^+ samples was used. First the samples were evacuated at room temperature for 10 min. Reproducibly a pressure of $1 \cdot 10^{-4}$ mbar was achieved. Then 130 mbar of the reducing gas was added and the samples heated to 240 °C. They were kept at this temperature for a certain time. The total time the samples were heated (including the time needed to bring the temperature to 240 °C) is called reduction time. If not stated otherwise the reduction time is 15 min. The samples were then allowed to cool to room temperature with the reducing gas still present. Cooling

took about 120 min for CO and only 30 min for H_2 which has much better heat conductivity because of its smaller molecular weight.

APPARATUS

The chamber of the custom built high vacuum sample compartment for *in situ* luminescence experiments shown in Figure 1 is made entirely from stainless steel except where stated otherwise. Apart from the viton seal **VS**, copper and indium metal seals minimize contamination of the sample with hydrocarbon impurities. The sample **SA**, in our case a quartz plate coated with zeolite, is held in a small stainless steel cup. This cup is put into the sample holder **SH** made of copper. The sample is positioned at the intersection of the optical axis going through **W**, **W'**, $\mathbf{L_1}$ and $\mathbf{L_{2,3}}$. The sample holder **SH** can be moved with the metal bellow sealed linear motion feed through **MF** in order to compensate for a varying sample thickness. The sample holder is heated with the heating system **HS** made of thermocoax or cooled by the flexible thermal link **TL** made of copper-mesh to the cooltip **CT** which itself is in connection with an external liquid nitrogen dewar **D**. The temperature can be set from -100 to 450 °C and is monitored by a Pt100 resistor **TS**. To keep thermal losses low the sample holder **SH** is surrounded by a heat shield not shown in the figure. The chamber is mounted on the table at the backside flange **F**. Situated on this flange are all connections to the outside as the electrical feed through **EF**, a port **HV** leading to the high-vacuum pumping system, an insulated feed through which connects the cooltip **CT** with the liquid nitrogen dewar **D** and a separate port **PP** to purge the chamber. The front part of the chamber can be removed to gain access to the sample.

The high-vacuum pumping system consists of a 100 L/s turbomolecular pump (Alcatel 5100 PN), backed with a two-stage mechanical roughing pump (Alcatel 2004A). To minimize any contamination from the mechanical pump fluid a catalytic trap (Balzers URB 025) is put between the turbomolecular pump and the roughing pump. A pressure control unit (Balzers TPG 300) is used in connection with a pirani gauge (Balzers TPR 018) and a cold cathode gauge (Balzers IKR 020). The high-vacuum system is used as gas handling system as well. An additional absolute pressure gauge (MKS baratron type 122A, 111A readout) is used to measure defined amounts of reacting gas.

Luminescence spectra are measured using typically 2 mJ/shot of the third harmonic of a Nd:YAG laser (Continuum YG660A) as excitation source. The beam is dispersed on a quartz prism to isolate the 355 nm light. A $NaNO_2$ solution is used to set the exact laser power. The excitation beam was directed with a beam steering instrument through port **W** of the vacuum chamber onto the sample. The luminescence is collected with lens $\mathbf{L_2}$ which acts as window in the vacuum chamber and focused with lens $\mathbf{L_3}$ onto the circular input port of a quartz fibre bundle. The rectangular exit port of the bundle is focused on the entrance slit of a spectrograph (PARC HR320S, 137 g/mm ruled grating)

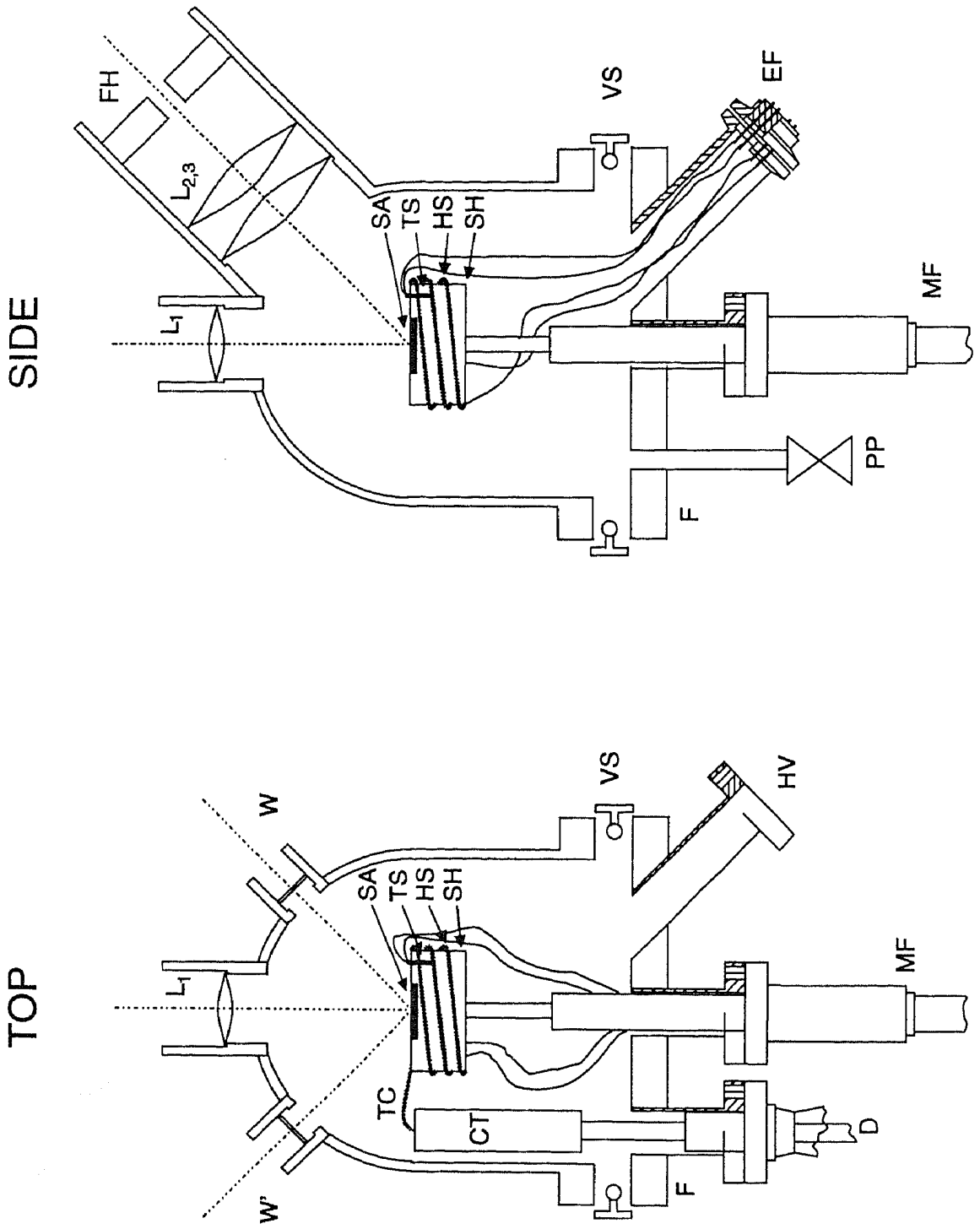

Figure 1. Top and side view of the *in situ* sample compartment. For an explanation see text.

with an optical system composed of two biconvex and one plane-convex cylindrical lens. The sample compartment is designed so as to allow also transient absorption measurements of solid samples. In this case the sample is excited either *via* **W** or *via* **W'**. To measure any change of absorption a flash of white light is focused onto the sample using $\mathbf{L}_1$. Again light is collected using $\mathbf{L}_{2,3}$.

As detector a gated OMA III system (EG&G PARC, 1455R-700-HQ detector, 1460/1462 controller, 1303 gate/delay generator, 1304 gate amplifier) is used. The various timing signals are generated with a four channel digital delay (Stanford Research Systems Inc. DG535) using the *trig.out* signal of the OMA III controller as a master trigger. Alternating spectrum scans and background scans are collected and the background corrected spectra are added. Spectrum scans are triggered by the laser pulse using the optical trigger input of the gate/delay generator while an electrical trigger signal is provided by the digital delay for the background scan. This trigger scheme implies that due to the delay of the electronics the first 125 ns of the decay of the luminescence are not measured. The reported spectra therefore do not conform to true steady state luminescence spectra because the fast components are missing. Typically 10 individual spectra each consisting of 250-1000 background corrected scans are measured in succession. This provides a good control of the stability of the sample. Manipulations, as for example, addition of water or evacuation are performed in the middle of the series. This allows the identification of even very small changes in the spectrum without doubt.

X-ray powder diffraction patterns of thin zeolite films were measured on a X-ray powder diffractometer (PADX) using non-filtered Cu-radiation (λ = 1.5406 Å) and a Ge-detector. The scan range was 2Θ = 4-90° in steps of 0.02° and the integration time per point was 5 s. A special sample holder for flat samples was used. Si served as internal standard in the determination of the unit cell parameters. The particle size was calculated from the full widths at halfheight (FWHH) of the diffraction peaks with the DECONV routing on the Stoe Powder Diffractometer System. The instrumental broadening was determined with strain free BaF_2.

Transmission electron micrographs were measured on a Hitachi H-600-2 electron microscope at 100 kV accelerator voltage. Chromium shadowed (50 Å, 45° incident angle) carbon replica were used.

RESULTS

Sample Characterization

In Figures 2 and 3 we report the X-ray powder diffraction pattern of 5 μm thick layers of Cu^{2+} exchanged zeolite A and zeolite X, respectively, for various co-cations. The 2Θ values, the peak intensities, and the Laue indices are listed in Tables 1 and 2.

From the comparison of the recorded diffraction patterns and the calculated unit cell parameters of the Cu^{2+} exchanged zeolites A and X (see Table 3) with the simulated powder diffraction patterns [48] and the known unit cell parameters of hydrated zeolite

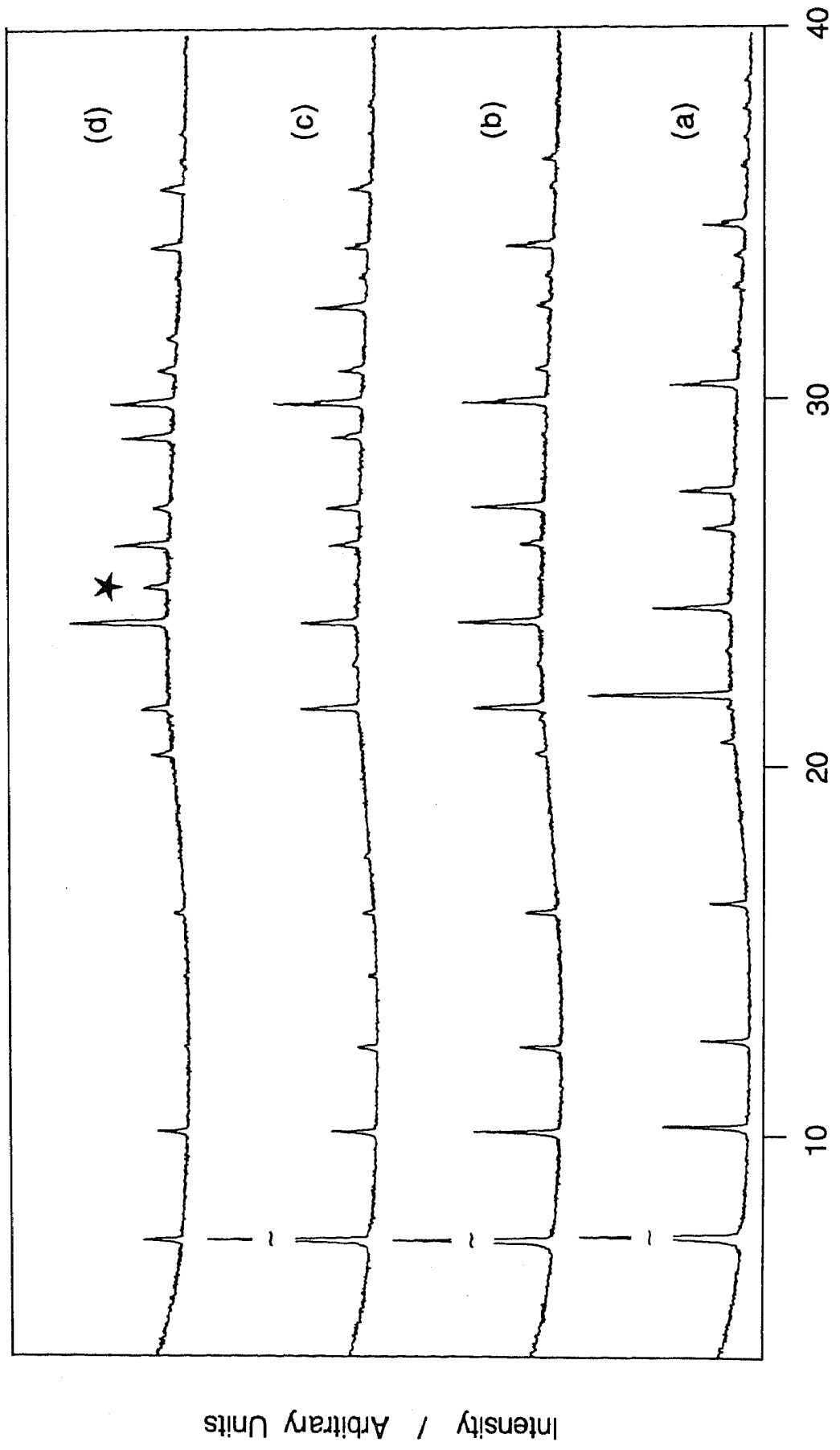

Figure 2. X-ray powder diffraction pattern of vinyl-LiCu-A (a), vinyl-NaCu-A (b), vinyl-KCu-A (c) and vinyl-CsCu-A (d) on glass support in the range of $2\Theta = 4\text{-}60°$. The additional peak with fractional indices 5, 4.5, 5 observed in vinyl-CsCu-A is indicated with a star. All patterns are scaled to (a).

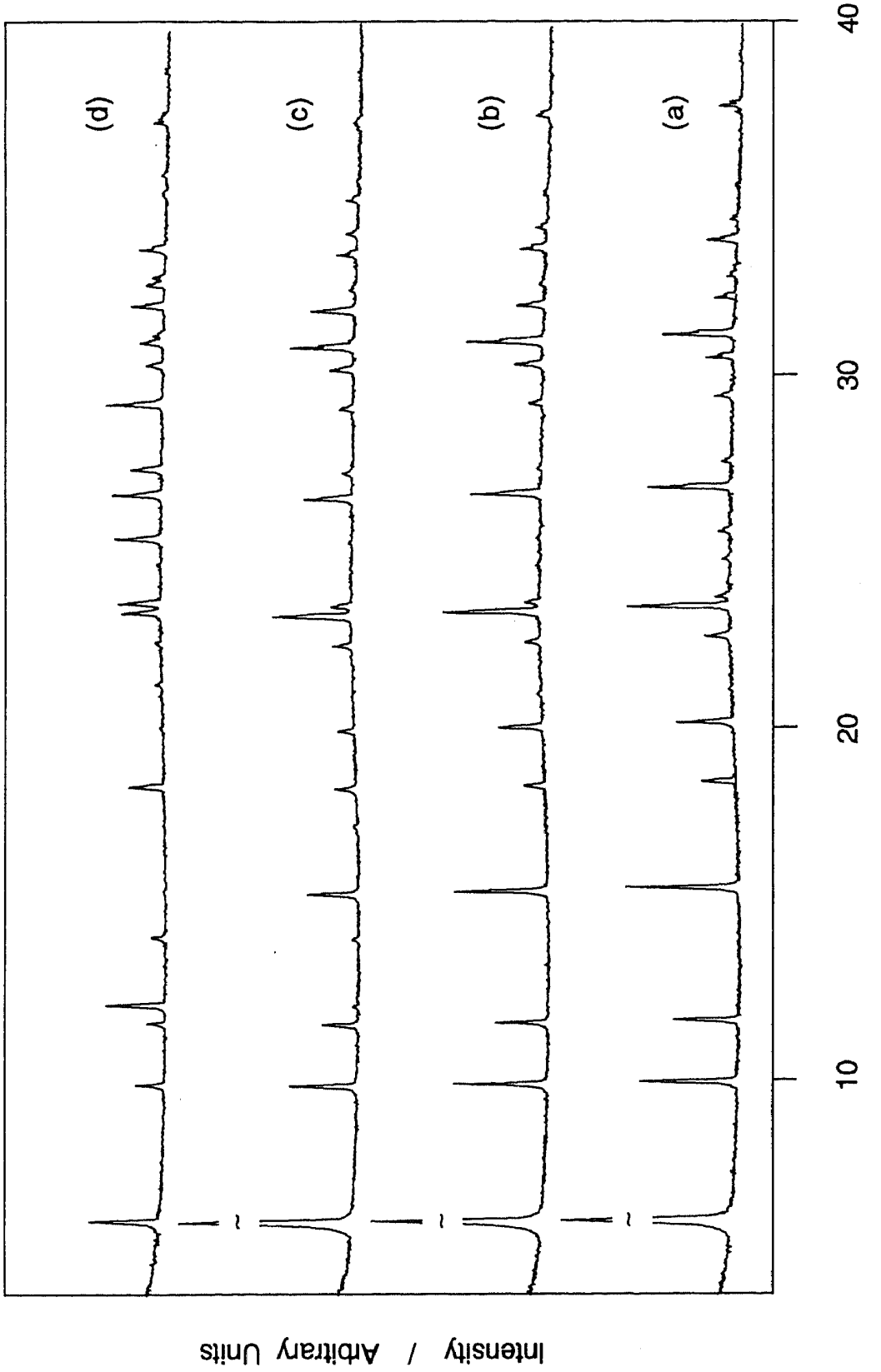

Figure 3. X-ray powder diffraction pattern of vinyl-LiCu-X (a), vinyl-NaCu-X (b), vinyl-KCu-X (c) and vinyl-CsCu-X (d) on glass support in the range of $2\Theta = 4\text{-}60°$. All patterns are scaled to (a).

Table 1
Intensities, 2Θ values and indices of vinyl-CuLi-A, vinyl-CuNa-A, vinyl-CuK-A and vinyl-CuCs-A. The 2Θ values are given up to 60°, as in [48]. The noise threshold for the peak finding program was 5.0 in all cases.

LiCu-A		NaCu-A		KCu-A		CsCu-A		
2Θ	Intensity	2Θ	Intensity	2Θ	Intensity	2Θ	Intensity	h k l
7.28	100	7.17	100	7.16	100	7.17	21	2 0 0
10.31	26	10.15	40	10.14	34	10.15	26	2 2 0
12.64	15	12.45	21	12.43	15			2 2 2
16.35	12	16.09	18	16.06	9	16.08	11	4 2 0
20.72	5	20.41	5			20.39	23	4 4 0
22.00	50	21.66	41	21.63	44	21.64	20	4 4 2/ 6 0 0
24.35	28	23.98	49	23.95	46	23.97	100	6 2 2
						24.91	29	[a]
26.51	13	26.11	14	26.07	25	26.09	53	6 4 0
27.53	20	27.11	44	27.07	27	27.09	18	6 4 0
				28.99	17	28.99	37	8 0 0
30.41	28	29.94	52	29.90	64	29.92	67	6 4 4/ 8 2 0
31.31	3	30.82	8	30.78	17	30.81	20	8 2 2/ 6 6 0
						31.68	9	6 6 2
33.04	3	32.54	9	32.50	35			8 4 0
33.89	4	33.37	5	33.32	6			8 4 2
34.71	17	34.18	30	34.13	15	34.16	34	6 6 4
36.31	3	35.75	4	35.71	14	35.73	24	8 4 4
		41.51	5	41.47	15	41.50	17	8 8 0
44.87	31	44.16	15	44.11	9	44.12	31	12 0 0/ 8 8 4

Table 1 continued

LiCu-A		NaCu-A		KCu-A		CsCu-A		
2Θ	Intensity	2Θ	Intensity	2Θ	Intensity	2Θ	Intensity	h k l
48.07	4							10 8 0/ 8 8 6
53.46	6	52.59	12	52.53	13	52.57	16	10 10 0/ 14 2 0
55.16	4	54.26	5	54.21	8	54.25	12	12 8 2/ 14 4 0
						57.51	7	14 6 2/ 10 10 6

[a]Not indexed in the given unit cell of CsCu-A.

Table 2

Intensities, 2Θ values and indices of vinyl-CuLi-A, vinyl-CuNa-X, vinyl-CuK-X and vinyl-CuCs-X. The 2Θ values are given up to 60°, as in [48]. The noise threshold for the peak finding program was 10.0 for Cs, Li-X and 5.0 in other cases.

LiCu-X		NaCu-X		KCu-X		CsCu-X		
2Θ	Intensity	2Θ	Intensity	2Θ	Intensity	2Θ	Intensity	h k l
6.15	100	6.11	100	6.07	100	6.10	89	1 1 1
10.06	20	9.99	22	9.94	18	9.98	42	2 2 0
11.81	13	11.73	13	11.66	10	11.72	25	3 1 1
				14.08	2	14.15	22	4 0 0
15.55	25	15.44	25	15.36	16			3 3 1
18.56	8	18.43	6	18.34	7	18.42	56	5 1 1/ 3 3 0
20.23	14	20.09	13	19.98	6			4 4 0
22.65	6	22.49	5	22.37	7			6 2 0
23.50	26	23.33	29	23.21	27	23.31	66	5 3 3

Table 2 continued

LiCu-X		NaCu-X		KCu-X		CsCu-X		
2Θ	Intensity	2Θ	Intensity	2Θ	Intensity	2Θ	Intensity	h k l
23.77	3	23.60	4	23.49	7	23.59	72	6 2 2
24.85	2							4 4 4
25.63	3					25.43	83	5 5 1
26.88	22	26.69	22	26.55	17	26.66	90	6 4 2
27.60	3			27.23	3	27.38	54	7 3 1
29.46	4	29.25	5	29.09	5	29.22	100	7 3 3
30.56	7	30.34	9	30.19	9	30.32	29	8 2 2/ 6 6 0
31.21	20	30.99	25	30.82	23	30.96	41	5 5 5/ 1 5 7
						31.17	15	6 6 2
32.26	6	32.03	9	31.87	17	32.01	63	8 4 0
32.87	2			32.47	3	32.62	35	7 5 3/ 9 1 1
						32.81	22	8 4 2
33.88	8	33.64	8	33.46	7	33.61	48	6 6 4
34.47	2	34.23	3	34.05	4			9 3 1/ 1 3 9
37.67	6	37.39	5	37.20	2	37.19	28	6 6 6/ 10 2 2
				40.64	5			8 8 0
						46.50	14	12 4 2
						51.69	22	10 10 0/ 14 2 0
53.64	2	53.25	2					11 9 3
				57.18	2			11 11 1/ 13 7 5/ 9 9 9

A [49] and X [50] we conclude that the frameworks of zeolites A and X are not destroyed by the cation exchange procedure applied by us. The quality in terms of intensities and peak widths of the obtained powder diffraction patterns of zeolites A and X as thin layers on glass support is unexpectedly good and allows even Rietveld refinement.

A sharp increase of the unit cell size listed in Table 3 is observed when going from the Li^+ - to the Na^+ - form, a smaller one from Na^+ - to K^+ - and possibly a decrease from the K^+- to the Cs^+ - sample. The latter decrease may be explained by the incomplete Cs^+ - exchange which may lead to a synergistic effect of optimal space filling with Na^+ exclusively on the small and Cs^+ on the large sites. An additional peak at $2\Theta = 24.913°$ is observed in the pattern of vinyl-CsCu-A. But it is not clear whether it belongs to the zeolite or to another phase. On the basis of a lattice constant of a = 24.601 it cannot be indexed by integer numbers. According to the literature, Cs^+ cations can occupy the positions (x,x,x) (C_3 symmetry) and/or (0, 1/4, 1/4) (D_{4h} symmetry) in zeolite A (space group $Fm\bar{3}c$) [51-55]. The appearance of the mentioned additional reflexion may indicate an ordered occupation of the Cs^+ deficient positions lowering the symmetry in the vinyl-CuCs-A.

A relative measure of the crystallinity of the samples can be derived from the relative intensity of the background due to the amorphous glass support. This gives the best crystallinity for the K^+ derivatives in both the A and the X series.

The particle sizes do not change in the series vinyl-LiCu-A (170 nm), vinyl-NaCu-A (163 nm), vinyl-KCu-A (170 nm) and vinyl-CsCu-A (174 nm). The same holds for series vinyl-LiCu-X (152 nm), vinyl-NaCu-X (140 nm), vinyl-KCu-X (145 nm) and vinyl-CsCu-X (159 nm). The small deviations lie within the experimental error. This is an additional indication that the method used for the exchange of cations is mild and does not lead to a destruction of the zeolite framework.

Table 3
Unit cell parameters *a* (Å) of Cu^{2+} exchanged zeolites A and X for the different co-cations.

	Li^+	Na^+	K^+	Cs^+
Zeolite A	24.220(1)	24.5918(0)	24.620(1)	24.601(2)
Zeolite X	24.796(1)	24.9704(9)	25.097(1)	24.9892(9)

No sign of Cu^{2+} in the form of precipitated $Cu(OH)_2$ on the outer surface of the zeolite crystals has been found so far. Transmission electron micrographs (carbon replicas) were measured before and after the reaction to acquire further information on

the influence of the Cu^{2+} ion exchange. In Figure 4 we present as typical examples results for K^+-A and K^+-X before and after Cu^{2+} exchange. The other samples showed very similar results. For zeolite A the well known cube-like crystals were found prior to the partial Cu^{2+} exchange. Some crystals of the alkali cation exchanged samples already showed a clearly visible corrugation of the surfaces which is more pronounced after the ion exchange with Cu^{2+}. Some crystals even lost their cube-like morphology. This finding is in accordance with the fact that attempts to achieve complete Cu^{2+} exchange in zeolite A resulted in a complete destruction of the zeolite framework and the formation of an unidentified product [56]. Zeolite X samples exhibit generally well-shaped triangular or hexagonal crystals with a clean surface prior to the Cu^{2+} exchange.

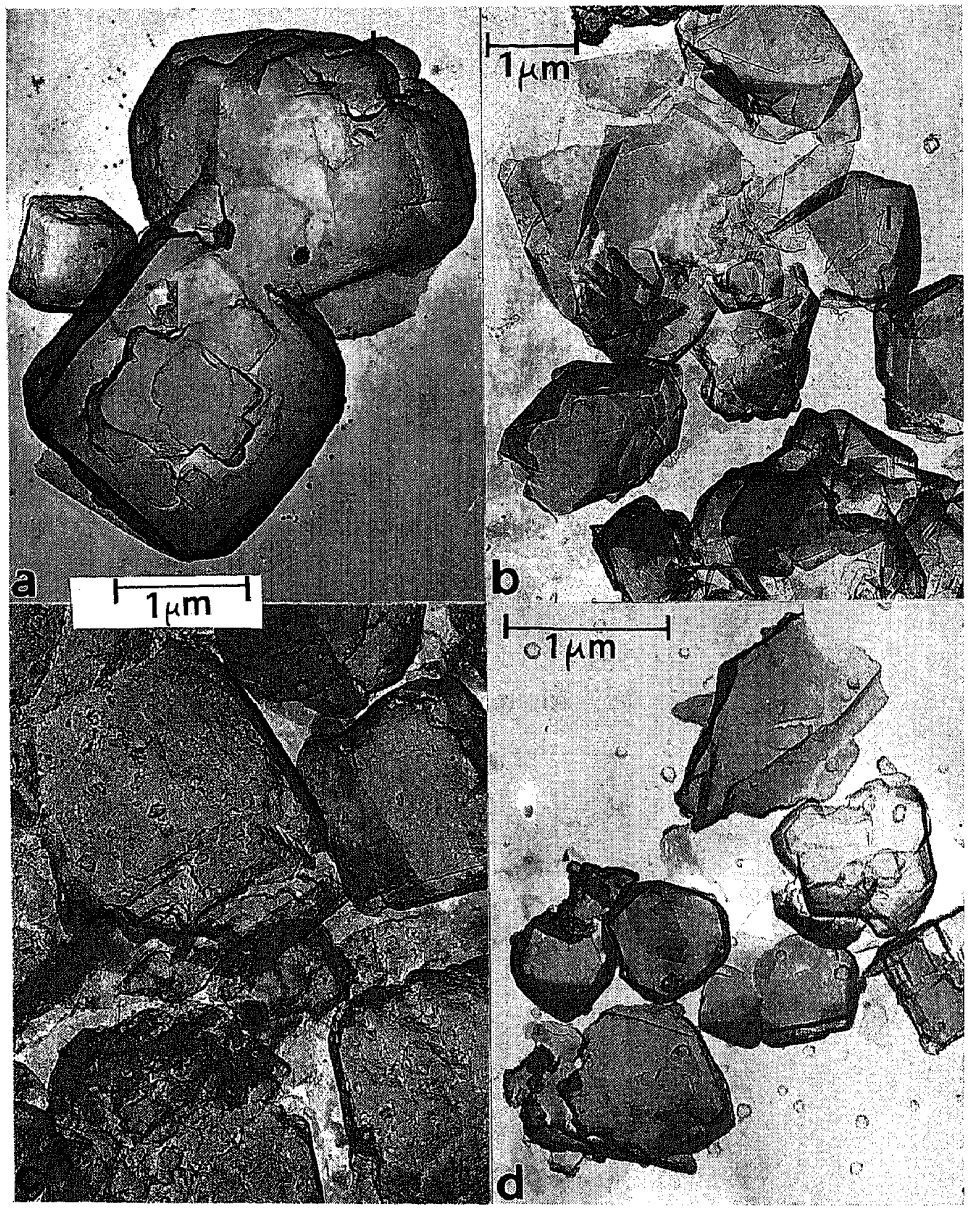

Figure 4. TEM micrographs of K^+-A (a), vinyl-CuK-A (c), K^+-X (b), and vinyl-CuK-X (d).

The morphology of these crystals is not changed by partial Cu^{2+} exchange. Some of the crystals, however, do now exhibit slightly corrugated surfaces similar to those observed on zeolite A samples. These measurements lead to the same conclusions as the powder diffraction patterns, namely that Cu^{2+} is incorporated in the zeolites by ion exchange of the charge compensating alkali cations.

The appearance of the corrugated surfaces could be due to partial hydrolysis of the zeolite surface. Si rich zeolites tend to be less prone to acid hydrolysis than Al rich zeolites. This seems to explain the more pronounced corrugation of the Al rich zeolite A. The crystals of both zeolite types are more affected by the exchange with Cu^{2+} than by exchange with different alkali cations. It is reasonable to assume that equilibria of the following type play a role in this surface reaction.

$$[Cu^{2+}(H_2O)_n]^{2+} \rightleftharpoons [Cu^{2+}(H_2O)_{n-1}OH^-]^+ + H^+$$

$$[Cu^{+}(H_2O)_{n-1}OH^-]^+ \rightleftharpoons [Cu^{+}(H_2O)_{n-2}(OH^-)_2]^+ + H^+$$

It appears reasonable to assume that the destruction of zeolite A observed at high Cu^{2+} loading is provoked by the specific coordination geometry preferred by Cu^{2+} which causes a distortion of the zeolite oxygen framework. Once the Cu^{2+} concentration exceeds a certain extent the distortion forces become so large that the crystal breaks. The more open structure of zeolite X seems to be less affected by this process, hence much higher exchanged samples are still stable. It is not clear, however, if the distortions are introduced by Cu^{2+}-O (framework) interactions or by formation of $[Cu(H_2O)_n]^{2+}$ complexes.

In conclusion, the samples investigated by us are fully crystalline and in some cases only the morphology of the surface has changed to a certain extent. Cu^{2+} is solely incorporated in the zeolites by stochiometrical exchange with charge compensating alkali cations at low exchange levels. In addition to the experiments described above this was verified to be the case up to about 20% Cu^{2+} (zeolite X) by AAS analysis of a series of Cu^{2+} zeolites with different degrees of exchange [38]. No traces of precipitated $Cu(OH)_2$ could be detected either by X-ray powder diffraction or TEM micrographs.

Luminescence Measurements

In Figure 5 we report typical emission spectra obtained with CO and H_2 reduced vinyl-CuCs-A and vinyl-CuCs-X. We show the spectra of Cs^+ samples because they exhibit

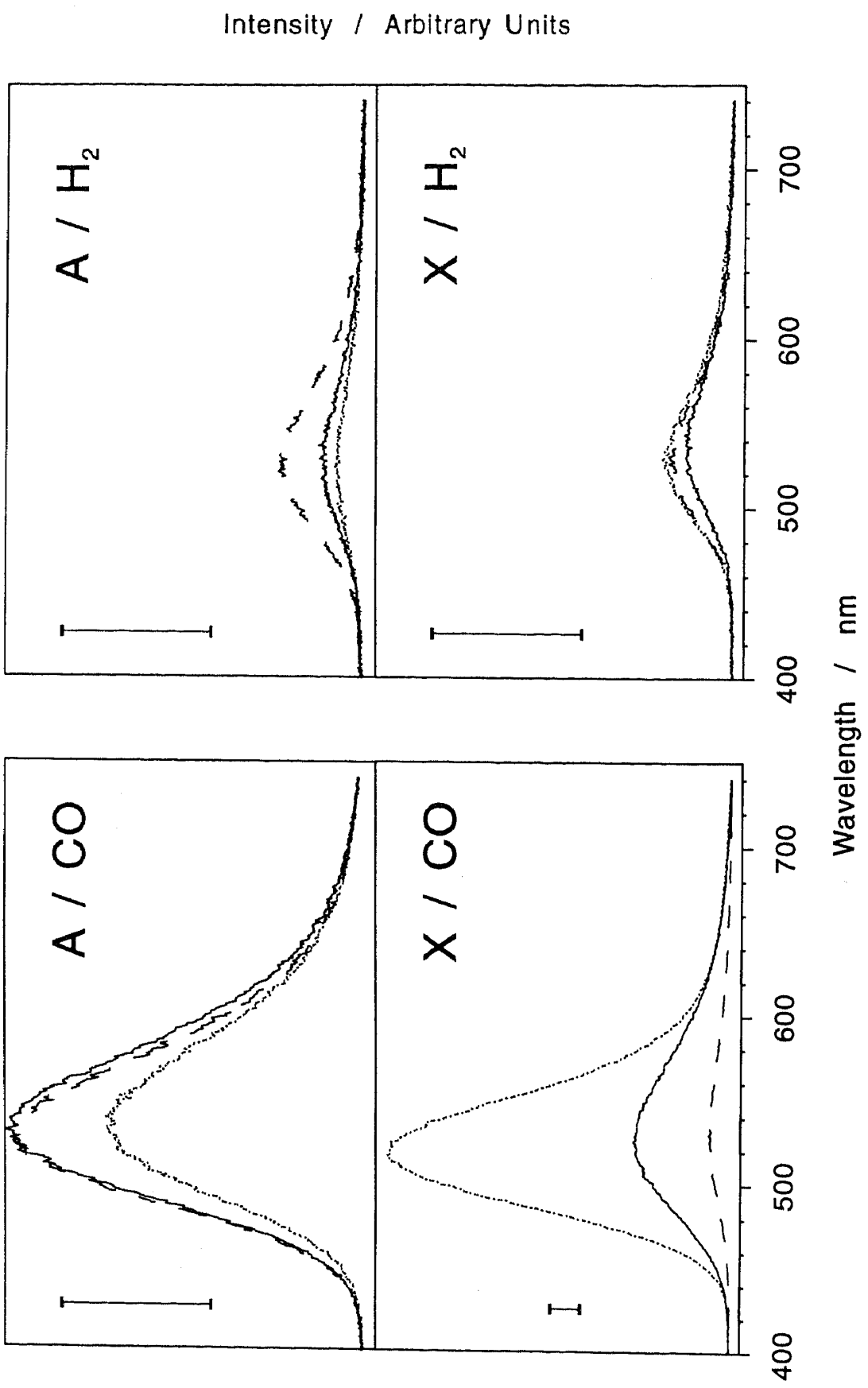

Figure 5. Typical luminescence spectra of CO reduced (left) and H_2 reduced (right) vinyl-CuCs-A (top) and vinyl-CuCs-X (bottom). For each sample three individual spectra corresponding to the sample still in the reducing gas (———), after 30 min of evacuation (- - -), and after the addition of 15 mbar of H_2O ···· are shown.

Table 4

Peak maxima and relative emission intensities of CO reduced and H_2 reduced vinyl-Cu-A and vinyl-Cu-X for different co-cations. Data are given for the sample after the reduction still in the reducing gas, after evacuation for 30 min, and after admission of *ca.* 15 mbar of H_2O.

Sample/ Reducing Gas	Peak Maxima (nm) and Relative Intensity					
	In the Reducing Gas		After Evacuation for 30 min		After Addition of 15 mbar of H_2O	
vinyl-CuLi-A/CO	515	0.6	509	0.8	523	0.6
vinyl-CuNa-A_{ut}/CO[b]	518		525		-	
vinyl-CuK-A/CO	532	1.9	532	37.7	532	0.9
vinyl-CuCs-A/CO	532	13.7	527	13.7	534	9.9
vinyl-CuLi-X/CO	[a]		[a]		534	1.2
vinyl-CuNa-X/CO	545	0.3	538	0.8	529	3.4
vinyl-CuK-X/CO	[a]		536	2.0	529	16.0
vinyl-CuCs-X/CO	527	19.4	533	4.0	519	68.3
vinyl-CuLi-A/H_2	[a]		[a]		[a]	
vinyl-CuNa-A_{ut}/H_2	~500 (sh) 605		497 628		-	
vinyl-CuK-A/H_2	[a]		530	0.6	~535	0.3
vinyl-CuCs-A/H_2	526	1.7	524	3.3	525	1.2
vinyl-CuLi-X/H_2	546	1.9	539	0.4	537	1.2
vinyl-CuNa-X/H_2	530	100.0	535	19.7	530	18.4
vinyl-CuK-X/H_2	536	3.2	~540	0.3	533	2.0
vinyl-CuCs-X/H_2	536	1.9	534	2.0	530	2.7

[a]No luminescence detectable.

[b]Measured on pellets, intensities are not comparable.

sufficient luminescence intensity in all cases. The reduction was performed after the standard pretreatment described above. In each case three spectra are shown, namely, the sample still in the reducing gas, after 30 min of evacuation, and after admission of H_2O. A single, well measurable, broad green emission band is observed for all samples. The peak maxima and the relative emission intensities are reported in Table 4. We immediately note that H_2 reduced samples exhibit a much less intense emission than CO reduced samples. This is found to be general with the exception of vinyl-CuNa-X which exhibits a stronger emission when reduced with H_2. Because of the mostly low emission intensities of H_2 reduced samples it was not possible to measure vinyl-CuLi-A and vinyl-CuNa-A. It was therefore not possible to verify the behaviour of H_2 reduced CuNa-A [38] but it should be stressed that this is the only sample where two emission maxima occur. As a rule Cu^+ zeolite X shows a somewhat less broad and more intense emission in comparison to Cu^+ zeolite A. Upon evacuation and upon admission of H_2O we find changes in the intensity of the emission that are sometimes rather drastic but that are accompanied by only minor shifts of the position of the peak maxima.

In Figures 6 and 7 we demonstrate the intensity dependence of the luminescence on the degree of hydration. A H_2 reduced sample of vinyl-CuNa-X is chosen because of its high emission intensity. The same dependence of the emission intensity on the water content of the sample is observed in CO reduced samples. CO has, however, the ability to quench the Cu^{+*} emission to some extent. The first spectrum in Figure 6 was taken after evacuating the reduced sample for 30 minutes at room temperature. Each of the next four spectra was collected after addition of the indicated amount of H_2O. The pressure in the last of these four spectra corresponds approximately to water vapour saturation of the sample. After this spectrum the sample was evacuated for 30 minutes at room temperature and the second cycle was started. The H_2O pressure indicated on the right side of each spectrum does not correspond to the equilibrium pressure because some parts of the sample compartment do absorb fair amounts of water, a process that is slow. The pressure readings are all taken under the same conditions, however, so that the relative numbers are representative. The open circles in Figure 7 correspond to the spectra in Figure 6 while the filled circles correspond to the independent experiments performed on another sample. The same overall behaviour has been found in the other samples. The maximum emission intensity occurs for different zeolites and different co-cations at a different water vapour pressure.

The high reactivity of Cu^{2+} zeolite towards reduction can be studied by measuring the emission intensity as a function of the reduction time. In a typical experiment on vinyl-KCu-A thin layers the normal pretreatment was applied followed by addition of 130 mbar CO. The samples were then heated in presence of this CO for different times up to 900 s. All of the samples were kept in CO for a total time of 4 h. Samples that were heated for 180 s and 900 s reached a final temperature of 240 °C. The temperature was lower for shorter heating times. Remarkably also samples that were kept in CO at room temperature only for 4 h exhibit a weak but measurable emission. This shows the high reactivity of Cu^{2+} zeolites towards CO. Samples treated at room temperature only show

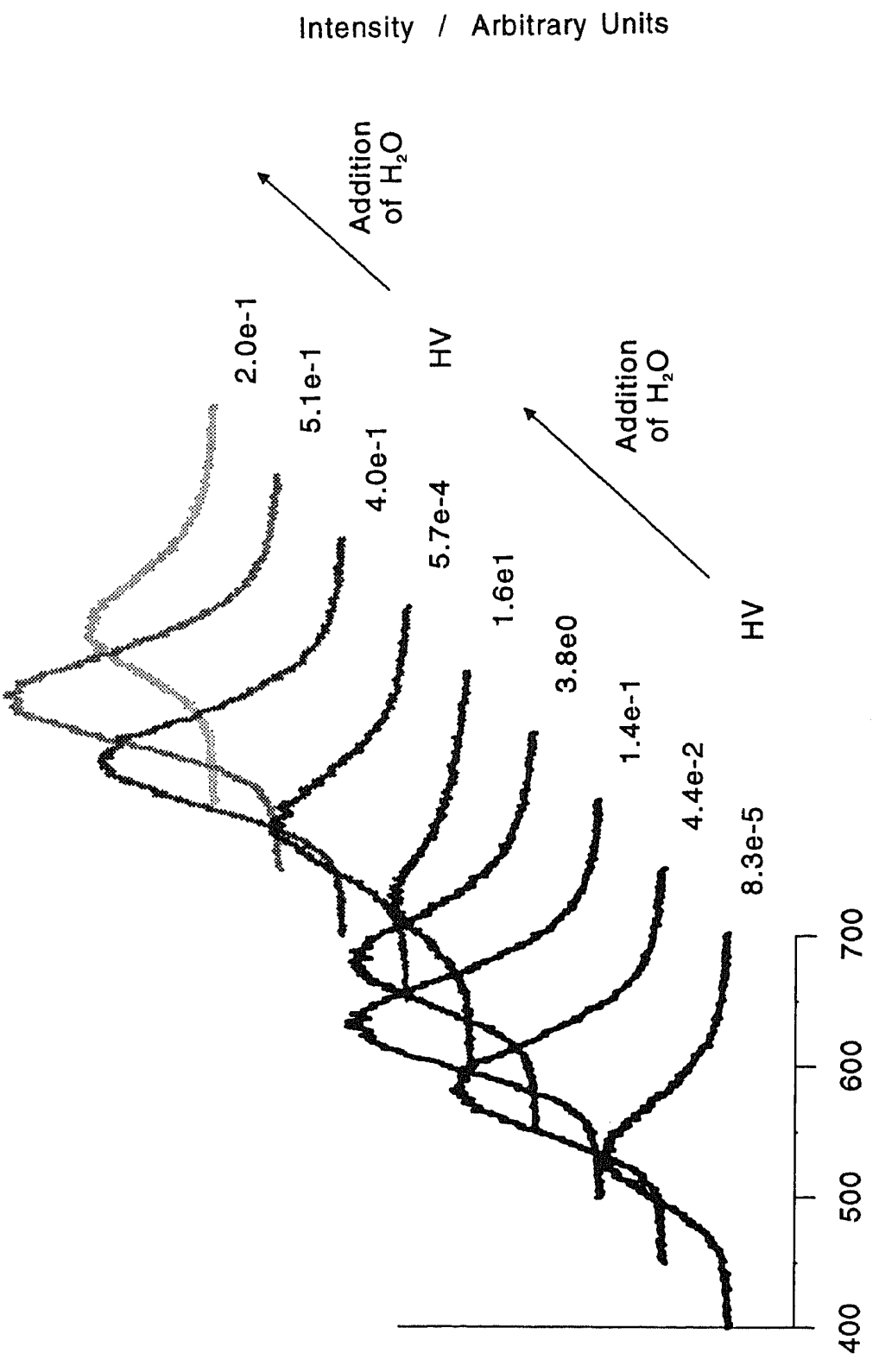

Figure 6. Luminescence spectra of vinyl-CuNa-X (exchanged 21.2%) as function of the degree of hydration. Two evacuation ——— hydration cycles are shown. On the right side of each spectrum the pressure in the sample compartment is indicated. This is taken to be equal to the water partial pressure. HV means 30 min of evacuation at room temperature.

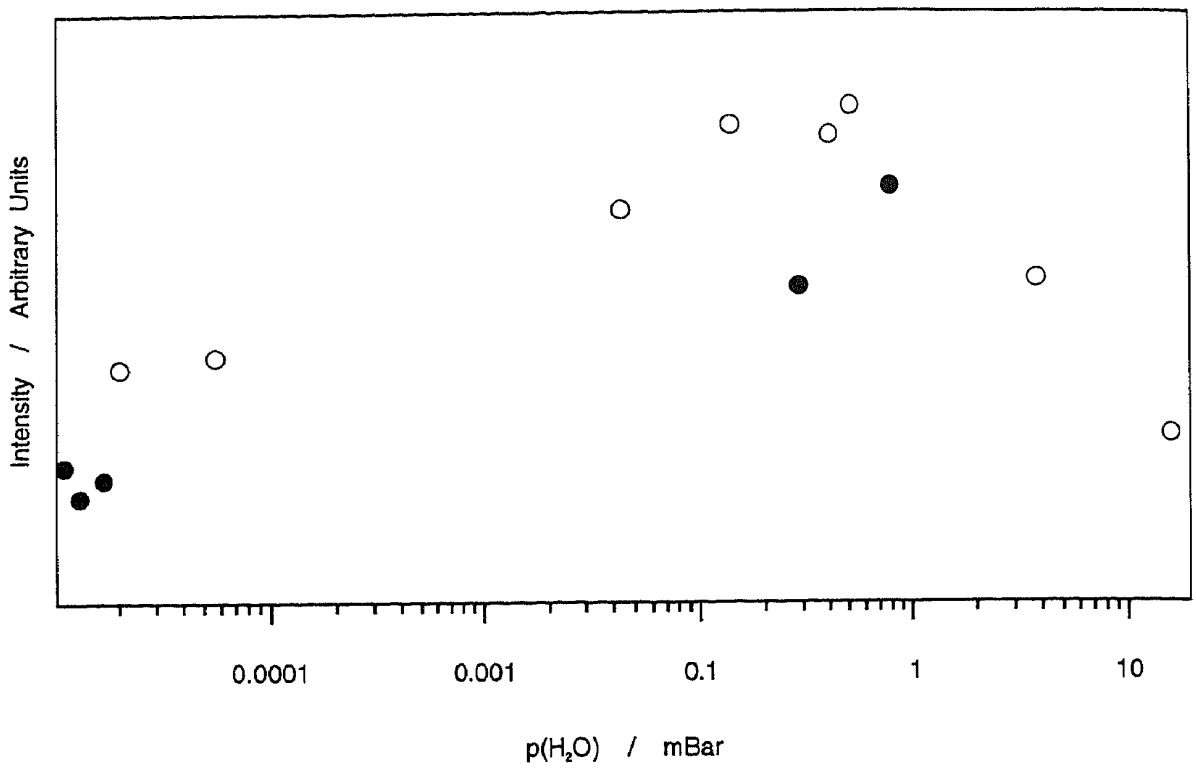

Figure 7. Luminescence intensity of vinyl-CuNa-X (exchange 21.2%) as a function of the H_2O partial pressure. Filled and empty circles denote two different samples.

a blue shift of 10 nm with respect to those heated for 900 s. The peak maxima and the relative emission intensities observed are: 536 nm/100(900 s), 533 nm/25(180s), 527 nm/7.5(75 s) and 526 nm/1.5(0 s).

To study the room temperature reactivity towards H_2 we measured the luminescence of the whole series from vinyl-LiCu-A to vinyl-CsCu-A in presence of H_2 for 4 h. Approximately 1 mm thick pellets were used in these experiments because H_2 reduced samples as a rule emit only weakly. After 4 h in 130 mbar H_2 all samples showed a barely detectable emission around 530 nm. We conclude that some reduction of Cu^{2+} zeolite A by H_2 takes place at room temperature.

According to Eq. (2) H_2O is consumed during the reduction of Cu^{2+} zeolites with CO. The influence of the water content on the reduction kinetics can be studied by measuring the luminescence of samples that have been evacuated for different times at different temperatures e.g. ranging from 5 min at room temperature to 90 min at 50 °C prior to the reduction. This allows the setting of the initial water contents of the samples prior to the reduction over a wide range. As an example we have observed a steady decrease in luminescence intensity the more the samples were dehydrated prior to the reduction. Samples that were evacuated for 90 min at 50 °C exhibit only about 50% of the emission intensity of samples that were evacuated for 5 min before being reduced. Evacuation for 30 min at room temperature corresponds to approximately the same water

content as evacuation for 15 min at 50 °C as can be seen from the almost equal emission intensities of the corresponding samples.

DISCUSSION

Stability of Zeolites A and X towards Cu^{2+}

We have found that Cu^{2+} exchange of alkali zeolites by only a few percent does not affect the crystallinity of both zeolites A and X. Some changes of the morphology of the surface of the crystals caused by Cu^{2+} exchange have been observed. It is known, however, that zeolite A is not stable towards high Cu^{2+} exchange. The coordination of Cu^{2+} can be described in terms of distinct, rigid polyhedra while the alkali cations exhibit less well defined and less rigid coordination polyhedra [57-60]. It seems therefore that strain is induced in the zeolite framework upon exchange of the alkali ions by Cu^{2+}. This strain increases with increasing exchange level until the framework ruptures. The more loose framework of zeolite X can compensate better for this strain that the more compact zeolite A. Zeolite A therefore supports a lower degree of Cu^{2+} exchange only.

Electronic Structure of Cu^+ Zeolites

Theoretical studies of the electronic structure of Cu^+-exchanged zeolites have lead to the result that the first electronic absorption is due to a $Cu^+ \leftarrow$ zeolite-oxygen lone pair LMCT transition. Such a transition causes a formal reduction of Cu^+ to Cu^o and oxidation of the oxygen lone pair region of the zeolite denoted as (| $\circ\!<$). The HOMO region of the zeolite framework consists of many closely spaced localized states strongly concentrated on the oxygen atoms. In our early studies the energy of the HOMO remained very uncertain and we were therefore not able to make a sufficiently good estimate of the energy difference between the HOMO and the empty $4s^*$ orbital of the Cu^+ ion. This problem has been solved in the meantime. We know that the edge of the (| $\circ\!<$) levels is at about -10.7 eV [7]. This allows the construction of a correlation diagram based on good experimental information. To do this we assume a sufficiently diluted Cu^+ zeolite in which no Cu^+-Cu^+ interactions occur. The positions of the 3d, the 4s and the 4p levels of the free Cu^+ ion can be derived from the valence state ionization potential (15.3 eV) [3], from the first ionization potential (7.7 eV), and from the energy difference $E(Cu_{3d10\ 4p1})$-$E(Cu_{3d10\ 4s1})$ (3.2 eV), respectively. We show on the left side of Figure 8 the position of the Cu^+ levels, on the right side the relevant zeolite levels and in the middle the zeolite HOMO and LUMO levels with the $4p^*$, $4s^*$ and $3d^*$ orbitals of the Cu^+ in the zeolite. From our calculations it turns out that the 4s level of Cu^+ always interacts in an antibonding way with the zeolite HOMO. Therefore the $4s^*$ orbital is always destabilized by the amount Δ with respect to the 4s level. The magnitude of Δ may vary from site to site. The $4p^*$ and $3d^*$ orbitals are in brackets because their splitting depends on the geometry of the environment which is not sufficiently known and may

change significantly from site to site. Calculations have lead to the result, however, that the $3d^*$ levels always remain below the zeolite lone pair orbitals (| O<).

Based on this energy diagram the two charge transfer transitions $4s^* \leftarrow$ (| O<) and $4p^* \leftarrow$ (| O<) leading to excited states denoted as (| O<)$(4s^*)^1$ and (| O<)$(4p^*)^1$, respectively, have to be considered. To explain our experimental data only the first one is important. If the interaction of the Cu^+ ion with the zeolite is relatively weak so that the correlation diagram in Figure 8 is valid then the energy ΔE_{CT} for the $4s^* \leftarrow$ (| O<) transition is equal to the difference of the ionization potential IP((| O<)) of the oxygen lone pair (| O<), and the ionization potential IP(Cu) of the 4s electron of the copper atom plus a correction Δ which accounts for the strength of the interaction of 4s level with the zeolitic environment.

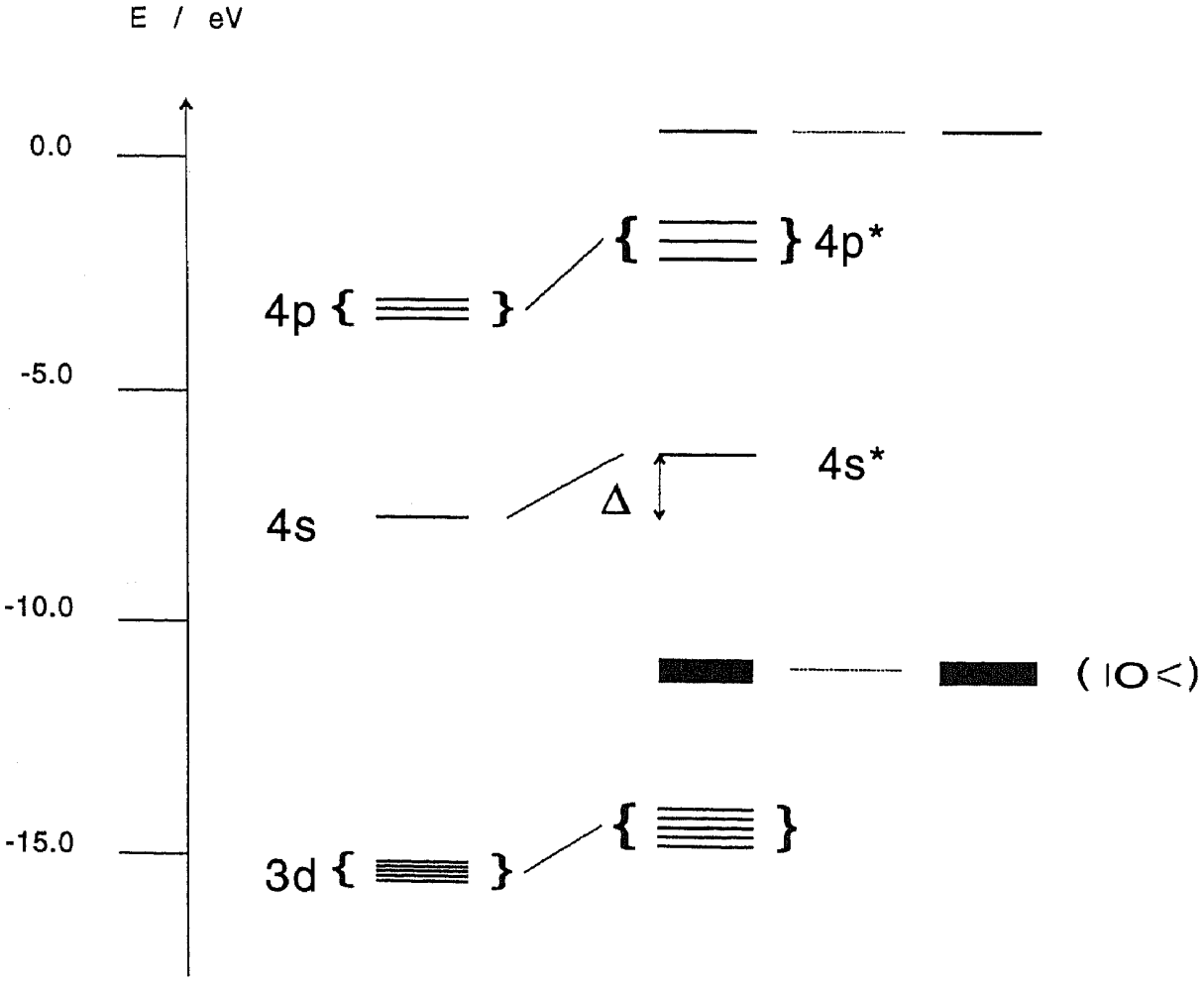

Figure 8. Correlation diagram of Cu^+ zeolites.

$$\Delta E_{CT}(Cu^+ \leftarrow (\ |\ o\lessdot)) = IP((\ |\ o\lessdot)) - IP(Cu) + \Delta \qquad (3)$$

A similar expression has been used to calculate the $5s^* \leftarrow (\ |\ o\lessdot)$ LMCT transition in Ag^+-A zeolites [8]. Inserting the numbers in equation (3) leads to $\Delta E_{CT}(Cu^+ \leftarrow (\ |\ o\lessdot)) = 10.7$ eV - 7.7 eV + Δ or to $\Delta E_{CT}(Cu^+ \leftarrow (\ |\ o\lessdot)) = 413$ nm - $|\ \Delta\lambda\ |$. This is in agreement with the observation that the edge of the first electronic transition in copper zeolites lies at about 370 nm. The large Stokes shift observed between absorption and emission can be explained to be due to its charge transfer character. Comparing the ionic radii of Cu^+ (0.96 Å) and Cu^0 (1.1 Å) we expect a large geometrical relaxation in the excited state and therefore a large Stokes shift.

Influence of the Co-cation

The interpretation of the electronic structure of Cu^+ zeolites forwards an explanation of the influence of the co-cation on the luminescence. The size of the unit cell is influenced by the ionic radius of the co-cation giving rise to a smaller unit cell, i.e. a more compact zeolite framework for small co-cations. The size of the unit cell is, however, not expected to be influenced by the reduction of Cu^{2+} to Cu^+ at our low exchange levels despite the large difference between the ionic radii of Cu^{2+} and Cu^+. A more compact zeolite framework gives rise to a shorter interaction distance of Cu^+ with the zeolite oxygens resulting in a larger Δ. We therefore expect a blue shift of the absorption edge and of the emission maximum. We find indeed a correlation in the case of the CO reduced zeolite A samples, independent of their measurement in the presence of CO, under evacuation or the rehydrated state. For these samples we find a steady red shift with increasing size of the unit cell. Insufficient data are available to decide on the quality of the correlation for H_2 reduced zeolite A layers. No correlation has been observed in zeolite X independently if the samples are reduced with CO or with H_2. We can imagine two different explanations for the different behaviour of the Cu^+-exchanged zeolite A and zeolite X. First, in zeolite A only equivalent sites are occupied which *feel* the compression of the zeolite lattice in the same way while this seems not to be the case in zeolite X. Second, due to the looser structure of zeolite X the Cu^+ ions change sites upon the compression of the zeolite lattice i.e. occupy different sites depending on the co-cation. Lack of structural data on Cu^+ zeolites does not allow us to decide if and which of the two factors is important.

Influence of the Degree of Hydration on the Cu^+ Luminescence

Figures 6 and 7 show that the intensity of the Cu^+ emission is remarkably influenced by the degree of hydration of the samples. A well defined amount of water is needed to achieve maximum emission intensity. The optimum amount of water depends on the co-cation and on the type of zeolite. No correlation between these two parameters has been

found so far. Evacuation or addition of H_2O also results in small spectral shifts of typically 10 nm. The extent or the direction of the shift is not related to the structure of the zeolite or the co-cation. Addition or removal of H_2O can not promote any redox reaction, hence the dependence of the emission intensity on the H_2O vapour pressure does not reflect a change in Cu^+ concentration but an enhancement and an attenuation of different deactivation channels of Cu^{+*}. To explain the maximum in the luminescence intensity curve at a certain vapour pressure two different factors influencing the radiative emission must be forwarded. At low hydration addition of water increases the emission probability. Above a certain water content H_2O dominantly acts as a quencher. At present we can only speculate on the mechanisms involved. Nevertheless we suggest that the coordination of the first H_2O molecules enables the Cu^{+*} ion to adjust itself into a favourable coordination, the coordination environment becomes more rigid and therefore leads to an enhancement of the emission. At the same time Cu^{+*} is already surrounded by a certain number of OH oscillators. We propose that the Cu^{+*} couples to them and gets deactivated in a similar way as described for the deactivation of Eu^{3+*} in zeolite A and Y [61]. The overall effect is still an increase in luminescence if we assume that Cu^{+*} couples only weakly to the OH oscillators. If Cu^{+*} becomes surrounded by more water molecules in a second coordination shell deactivation is enhanced because of the increasing number of OH oscillators. We therefore arrive at a situation where at a low degree of hydration addition of H_2O increases the emission probability until a maximum is reached and further addition of H_2O results in a decrease of the emission probability.

Influence of the Reductant on the Luminescence Intensity

The change of the emission intensity observed when H_2 is removed by evacuation after the reduction has its origin solely in the decrease of the water content of the reduced sample. As we indicate in the previous paragraph the maximum emission intensity occurs at different degrees of hydration for samples with a different co-cation or a different type of zeolite. For a certain sample we do not know *a priori*, if after reduction the degree of hydration is above or below the optimum. We therefore expect to find samples which show an increase of the intensity upon removal of H_2, which causes also removal of H_2O, and other samples which show a decrease of the emission. For CO reduced samples a further complication arises because of the formation of Cu^+-CO complexes during or after the reduction. In these complexes static quenching of the Cu^{+*} emission is expected to occur [2]. The importance of both intensity determining processes, the degree of hydration of the zeolite and the static quenching of the Cu^{+*} emission by the formation of CO complexes, is nicely illustrated in Figure 5. Upon evacuation we find an increase of the emission for vinyl-CuCs-X due to the destruction of the Cu^+-CO complex. The removal of the quencher seems to be the dominating process in this case while for vinyl-CuCs-A we find a decrease in intensity. In the latter case the loss of H_2O seems to be the intensity determining process.

Factors Influencing the Reactivity of Cu^{2+} Towards Reduction - (i) Water contents of the sample prior to the Reduction.

From Eq. (2) we know that H_2O is being consumed in the reduction of Cu^{2+} with CO. We can therefore expect that the degree of reduction achieved in a CO reduced sample is eventually limited by the amount of H_2O available for the reduction. The degree of reduction can be directly monitored by the intensity of the Cu^{+*} emission if we keep all other intensity determining factors under control. In wet samples where enough water molecules are available near each Cu^{2+} ion we expect the reduction to be complete in a rather short time. In samples that are a little dryer enough water is still available but not necessarily in the direct neighbourhood of a Cu^{2+} ion. Reduction will then be slower because H_2O molecules have to diffuse to some of the Cu^{2+} ions in order to reduce them. We therefore expect less completely reduced samples after a certain time and therefore less emission intensity. In even more dehydrated samples the overall amount of water limits the number of Cu^{2+} ions that can be reduced. Complete reduction in this case is no longer possible. We can therefore control the degree of reduction and hence the luminescence intensity in CO reduced samples by controlling the number of water molecules available for the reduction.

The decrease of the emission intensity in samples that are more completely dried prior to the reduction with H_2 can not be understood on the same basis because no H_2O is consumed during the reduction according to Eq. (1). We have to conclude that H_2O strongly influences that reactivity of the system and is vital to the reduction even if it does not occur in the overall stoichiometry.

(ii) Influence of Reduction-Heating Time.

Because of the way the experiments with different heating times were performed it is not possible to determine without doubt the influence of the reduction time and the reductio temperature. The samples that were heated only for a short time did not reach the same temperature as the samples that were heated longer. However, the following interpretation seems to be reasonable. We note that the luminescence intensity of the sample is not linearly dependent on the reduction time; the reduction is much faster at higher temperatures. We therefore conclude that a significant energy of activation is involved. This results in an exponential dependence of the Cu^+ concentration upon the reduction temperature. For short reduction times where the samples do not reach a reduction temperature of 240 °C the reduction temperature is proportional to the reduction time. The reduction finally reaches its limiting speed and the Cu^+ concentration rises linearly with time. The limiting speed is probably controlled by diffusion of the reductant or of H_2O.

Acknowledgement

This work is part of project BBW-REN(88)28/EPA 217 and BBW-REN(91)28/EPA financed by the *Schweizerisches Bundesamt für Energiewirtschaft.*

REFERENCES

1. J. Texter, D.H. Strome, F.G. Herman, and K. Klier, J. Phys. Chem. **81**, 333 (1977).
2. J.H. Strome and K. Klier, J. Phys. Chem. **84**, 981 (1980).
3. G. Calzaferri and L. Forss, Chem. Phys. Lett. **103**, 296 (1984).
4. G. Calzaferri and L. Forss, Helv. Chim. Acta, **70**, 465 (1987).
5. G. Blasse, Adv. Inorg. Chem. **35**, 319 (1990).
6. G. Blasse, Structure and Bonding **76**, 153 (1991).
7. G. Calzaferri and R. Hoffmann, J. Chem. Soc. Dalton Trans. 917 (1991).
8. R. Beer, G. Calzaferri, J. Li, and B. Waldeck, Coord. Chem. Rev. **111**, 1489 (1991).
9. B. Elleuch, C. Naccache, Y. Ben Taarit, and G. Wicker, Stud. Surf. Sci. Catal. **19**, 139 (1989).
10. S. Bun, S. Nishiyama, S. Tsuruya, and M. Masai, Appl. Catal. **59**, 13 (1990).
11. M. Anpo, T. Nomura, T. Kitao, E. Ciamello, D. Murphy, M. Che, and M.A. Fox, Res. Chem. Intermed. **15**, 225 (1991).
12. M. Anpo. In: Photochemical conversion and Storage of Solar Energy, E. Pelizetti, M. Schiavello (Eds.). Kluwer Academic Publisher, Dordrecht, 1991.
13. M. Anpo, T. Nomura, T. Kitao, E. Ciamello, M. Che, and M.A. Fox, Chem. Lett. 889 (1991).
14. J.O. Petunchi and W.K. Hall, J. Catal. **80**, 403 (1983).
15. H. Hamada, N. Matsubayashi, H. Shiimada, Y. Kintaichi, T. Ito, and A. Nishijima, Catal. Lett. **5**, 189 (1990).
16. M. Iwamoto, H. Yahiro, K. Tanda, N. Mizuno, Y. Mine, and S. Kagawa, J. Phys. Chem. **95**, 3727 (1991).
17. M. Iwamoto, H. Yahiro, Y. Torikai, T. Yoshioka, and N. Mizuo, Chem. Lett. 1967 (1990).
18. M. Iwamoto and H. Hamada, Catal. Today **10**, 57 (1991).
19. S. Kagawa, H. Ogawa, H. Furukawa, and Y. Teraoka, Chem. Lett. 407 (1990).
20. A.H. Badran, G.A. El-Shobaky, and M.M. Selim, Egyp. J. Chem. **24**, 319 (1981).
21. E.E. Miró, D.R. Ardiles, E.A. Lombardo, and J.O. Petunchi, J. Catal. **97**, 43 (1986).
22. H.S. Lee and K. Seff, J. Phys. Chem. **85**, 397 (1981).
23. H.S. Lee, W.V. Cruz, and K. Seff, J. Phys. Chem. **86**, 3562 (1982).
24. I.E. Maxwell and J.J. de Boer, J. Phys. Chem. **79**, 1874 (1975).
25. T. Ichikawa and L. Kevan, J. Chem. Soc., Faraday Trans. I, **77**, 2567 (1981).
26. T. Ichikawa and L. Kevan, J. Am. Chem. Soc. **103**, 5355 (1981).
27. L. Kevan and M. Narayana, Am. Chem. Soc. Symp. Ser. **218**, 283 (1983).
28. D. Packet and R.H. Schoonheydt, Stud. Surf. Sci. Catal. **18**, 41 (1984).
29. W.J. Mortier and R.A. Schoonheydt, Prog. Solid. St. Chem. **16**, 1 (1985).
30. M. Narayana and L. Kevan, J. Chem. Soc., Faraday Trans. **82**, 213 (1986).
31. M.W. Anderson and L. Kevan, J. Phys. Chem. **91**, 1850 (1987).
32. H. Feng, H. Baussart, M. Le Bras, and J.-M. Leroy, J. Chim. Phys. **86**, 2081 (1989).
33. R.A. Schoonheydt, J. Phys. Chem. Solids, **50**, 523 (1989).
34. T. Ichikawa and L. Kevan, J. Am. Chem. Soc. **105**, 402 (1983).
35. D. Packet and R.H. Schoonheydt, Stud. Surf. Sci. Catal. **28**, 385 (1986).
36. D. Goldfarb and K. Zukerman, Chem. Phys. Lett. **171**, 167 (1990).
37. J.D. Barrie, B. Dunn, O.M. Stafsudd, and P. Nelson, J. Lumin. **37**, 303 (1987).

38. R. Beer, G. Calzaferri, and I. Kamber, J. Chem. Soc., Chem. Commun. 1489 (1991).
39. D.W. Breck, Zeolite Molecular Sieves-Structure, Chemistry , and Use. John Wiley & Sons, New York, 1974.
40. A.H. Badran, J. Dwyer, and N.P. Evmerides, Inorg. Chim. Acta **21**, 233 (1977).
41. Y. Kurodaq, A. Kotani, H. Maeda, H. Moriwaki, T. Morimato, and M. Nagao, J. Chem. Soc. Faraday Trans. **88**, 1583 (1992).
42. Y. Kuroda, H. Maeda, H. Moriwaki, N. Bamba, and T. Morimoto, Physica B **158**, 185 (1989).
43. B.H. Wiers, R.J. Grosse, and W.A. Cilley, Environ. Sci. Technol. **16**, 617 (1982).
44. R.A. Schoonheydt, L.J. Vandamme, P.A. Jacobs, and J.B. Uytterhoeven, J. Catal. **43**, 292 (1976).
45. G. Calzaferri, K. Hädener, and J. Li, J. Chem. Soc., Chem. Commun. 653 (1991).
46. R. Beer, F. Binder and G. Calzaferri, J. Photochem. Photobiol. A; Chem. (1992), in press.
47. This is only one of the many possibilities to prepare zeolite monolayers or polylayers on surfaces. For other possibilities see G. Calzaferri, Proceedings, IPS 9, Beijing, 1992, in press.
48. R.V. Ballmoos, Collection of Simulated XRD Powder Patterns for Zeolites, Butterworth, 1984.
49. V. Gramlich and W.M. Meier, Z. Kristallogr. **133**, 134 (1971).
50. D.H. Olson, J. Phys. Chem. **74**, 2758 (1970).
51. W.J. Mortier, Compilation of Extra Framework Sites in Zeolites. Butterworth, 1982.
52. T.B. Vance and K. Seff, J. Phys. Chem. **79**, 2163 (1975).
53. R.R. Firor and K. Seff, J. Am. Chem. Soc. **99**, 6249 (1977).
54. V. Subramanian and K. Seff, J. Phys. Chem. **83**, 2166 (1979).
55. V. Subramanian and K. Seff, J. Phys. Chem. **84**, 2928 (1980).
56. I. Kamber, PhD thesis, Bern, 1992.
57. W. Bidell, V. Shklover and H. Berke, Inorg. Chem., in press.
58. V.A. Igonin, O.I. Schegolikhina, A.A. Zhdanov, V. Shklover, S.V. Lindeman, and Yu. T. Struchkov, J. Organomet. Chem., in press.
59. K. Smollander, Ann. Acad. Sci. Fennicae, **A200**, 1 (1983).
60. J. Gazo, I.B. Bersuker, J. Garaj, M. Kabesove, J. Kohout, H. Langfelderova, M. Melnik, M. Serator, and F. Valach, Coord. Chem. Rev. **19**, 253 (1976).
61. S.L. Suib, R.P. Zerger, G.D. Stucky, T.I. Morrison, and G.K. Shenoy, J. Chem. Phys. **80**, 2203 (1984).